IEEE Access
Multidisciplinary | Rapid Review | Open Access Journal

Received April 19, 2020, accepted May 2, 2020, date of publication May 6, 2020, date of current version May 20, 2020.

Digital Object Identifier 10.1109/ACCESS.2020.2992631

An Approach of One-vs-Rest Filter Bank Common Spatial Pattern and Spiking Neural Networks for Multiple Motor Imagery Decoding

HONGTAO WANG[1], (Member, IEEE), CONG TANG[1], TAO XU[1], TING LI[1], LINFENG XU[1], HONGWEI YUE[1], PENG CHEN[1], JUNHUA LI[1,3], (Senior Member, IEEE), AND ANASTASIOS BEZERIANOS[2,4], (Senior Member, IEEE)

[1]Faculty of Intelligent Manufacturing, Wuyi University, Jiangmen 529020, China
[2]Centre for Life Sciences, National University of Singapore, Singapore 117456
[3]School of Computer Science and Electronic Engineering, University of Essex, Colchester CO4 3SQ, U.K.
[4]Department of Medical Physics, University of Patras, 26504 Patras, Greece

Corresponding author: Hongtao Wang (nushongtaowang@qq.com)

This work was supported in part by the Natural Science Foundation of Guangdong Province under Grant 2018A030313882, in part by the Projects for International Scientific and Technological Cooperation under Grant 2018A05056084, in part by the National Natural Science Foundation of China under Grant 61806149, in part by the Guangdong Basic and Applied Basic Research Foundation under Grant 2020A1515010991, in part by the Jiangmen Brain-like Computation and Hybrid Intelligence R&D Center under Grant [2018]359 and Grant [2019]26, in part by the Science Foundation for Young Teachers of Wuyi University under Grant 2018td01, in part by the Innovation Training Foundation for Guangdong University Students under Grant 1081700308, and in part by the Innovation and Entrepreneurship Project of Wuyi University under Grant 3344100104.

ABSTRACT Motor imagery (MI) is a typical BCI paradigm and has been widely applied into many aspects (e.g. brain-driven wheelchair and motor function rehabilitation training). Although significant achievements have been achieved, multiple motor imagery decoding is still unsatisfactory. To deal with this challenging issue, firstly, a segment of electroencephalogram was extracted and preprocessed. Secondly, we applied a filter bank common spatial pattern (FBCSP) with one-vs-rest (OVR) strategy to extract the spatio-temporal-frequency features of multiple MI. Thirdly, the F-score was employed to optimise and select these features. Finally, the optimized features were fed to the spiking neural networks (SNN) for classification. Evaluation was conducted on two public multiple MI datasets (Dataset IIIa of the BCI competition III and Dataset IIa of the BCI competition IV). Experimental results showed that the average accuracy of the proposed framework reached up to 90.09% (kappa: 0.868) and 81.33% (kappa: 0.751) on the two public datasets, respectively. The achieved performance (accuracy and kappa) was comparable to the best one of the compared methods. This study demonstrated that the proposed method can be used as an alternative approach for multiple MI decoding and it provided a potential solution for online multiple MI detection.

INDEX TERMS Electroencephalogram, motor imagery (MI), filter bank common spatial pattern (FBCSP), spiking neural networks (SNN).

I. INTRODUCTION

Electroencephalography (EEG) signal is usually used in brain-computer interface (BCI) systems due to its high temporal resolution [1]. Motor imagery (MI)-based BCI is one of classical paradigms and has been employed to restore the communication pathway or movement function for disabled, paralyzed, and stroke patients [2], [3]. Patients are able to output their thoughts by only imagining without any real movements and speaking, as well as realising practical operations [4].

In the establishment of a BCI system, feature extraction is a crucial step. Common spatial pattern (CSP) is a widely used method to extract spacial features as it effectively constructs the best spatial filter for differentiating two classes of motor imagery. As CSP searches the best spatial filter by considering temporal dynamics, it depends on the information in the temporal domain and is sensitive to temporal noise. Common

The associate editor coordinating the review of this manuscript and approving it for publication was Li He.

TABLE 1. Description of multiple motor imagery datasets.

Datasets	Categories	Subject	Number of train	Number of test	Channel selection
Dataset IIIa	left hand, right hand, feet, and tongue	K3b K6b L1b	180 trials 120 trials 120 trials	180 trials 120 trials 120 trials	FT7,FC5,FC3,FC1,FCz,FC2,FC4,FC6,FT8, T7,C5,C3,C1,Cz,C2,C4,C6,T8,TP7,CP5,CP3, CP1,CPz,CP2,CP4,CP6,TP8,P3,P4,P6,PO4,PO6
Dataset IIa	left hand, right hand, feet, and tongue	A01-A09	288 trials per subject	288 trials per subject	FC3,FC1,FCz,FC2,FC4, C3,C1,Cz,C2,C4,CP3, CP1,CPz,CP2,CP4,P1,Pz,P2

spatial spectrum pattern (CSSP) was proposed to reduce the interference of such noise [5]. However, CSSP cannot offset the increased complexity of optimization problems because it increases the flexibility of the frequency filter with the delay taps. Afterwards, an improved algorithm was proposed, naming Common Sparse Spectral Spatial Pattern (CSSSP) [6].

Before applying CSP, a bandpass filter is usually used to concentrate on a specific frequency band. The specified frequency band largely affects the performance of CSP. In order to have good performance, frequency band is manually specified for each individual subject. Alternatively, a few frequency bands could be specified to extract features in different bands at the same time. Filter bank common spatial pattern (FBCSP) is one of such methods, extracting discriminative spatio-temporal information [7], [8]. Its variants were subsequently proposed, which are discriminative FBCSP (DFBCSP), sparse FBCSP (SFBCSP) and penalized time-frequency band CSP (PTFBCSP) [8]–[10]. These methods have different advantages. For example, DFBCSP allows to set subject-specific frequency band for filtering based on Fisher's ratio and has a better performance compared to FBCSP. SFBCSP automatically selects features in a few frequency bands based on the regression of the least absolute shrinkage and selection operator (LASSO). PTFBCSP overcomes the limitation of the fixed time period and fixed frequency band.

Spiking neural networks (SNN) has obtained a good classification effect as a classifier in the digital recognition, EEG-based motor imagery, and other classification problems [11]–[13]. Virgilio *et al.* used the original EEG signal, power spectrum density (PSD) and discrete wavelet transform (DWT) combined with SNN classifier to analyze and study the multiple-classes of motor imagery, and achieve a good classification effect [14]. Carino *et al.* conducted a taxonomic study by evaluating two different neuronal model coding strategies for two classes of motor imagery time-frequency characteristics in patients with brain death and healthy subjects [15]. Niranjani *et al.* used the spiking neural classifier based on the Online Meta-neuron based Learning Algorithm (OMLA) to classify MI. Due to the simultaneous use of global and local information of the network, the performance of the spiking neural classifier is better than other classifiers [16]. Salazar *et al.* demonstrated that the classification performance of spiking neural models (SNM) is a potential choice for EEG when training with fewer data samples [17]. Though the SNN has been applied in motor imagery analysis in the above literatures, the main contribution of this paper is to combine FBCSP with the SNN classifier for multiple MI decoding. The performance was evaluated using the dataset IIIa in the BCI Competition III and the dataset IIa in the BCI Competition IV [18], [19].

II. METHODOLOGY AND MATERIALS

A. DATA COLLECTION

We have evaluated our method on the dataset IIIa of the BCI Competition III and dataset IIa of the BCI Competition IV [18], [19]. More details of these multiple-class MI datasets are listed in Table 1. The channel selection for two datasets is based on the selection of channel location in [20]–[22]. These channels are selected mainly because they account for a higher proportion of MI information than other channels that have not been selected, and the channel selection range includes the brain activity areas of the four-classes of motor imagery. Choosing a small number of channels but a large proportion of the weight is beneficial to the subsequent processing speed of the entire experiment and improves the accuracy of multiple-classes of MI.

More specifically, the location of electrodes montage for two datasets are shown in Fig. 1 (red dots stand for the selected channels) and the numbers of channels for EEG collection are 60 and 22, respectively. For the dataset IIIa in BCI Competition III, there are three subjects and the paradigm consists of four MI tasks, namely left hand (class 1), right hand (class 2), both feet (class 3), and tongue (class 4). Each category has 90 trials for the subject K3b while 60 trials for the subjects K6b and L1b. For the Dataset IIa in the BCI Competition IV, there are nine subjects and four categories (left hand, right hand, foot and tongue). Each subject underwent two sessions, which comprised 6 runs separating by a short break. Each run had 48 trials with equivalent numbers for each class.

To analyze datasets, the experimental algorithm is run by using an Intel(R) Core(TM) i5 CPU @2.7 GHz host computer (Lenovo).

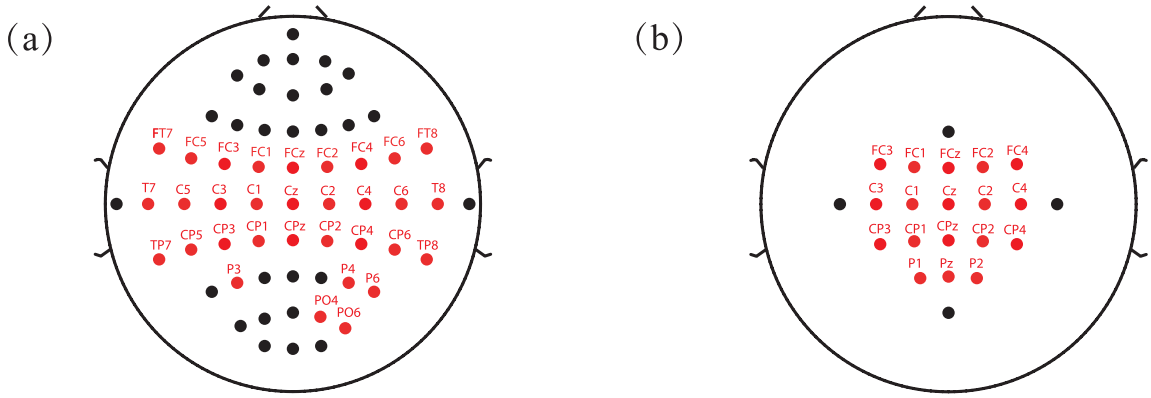

FIGURE 1. (a) and (b) are the placement of electrodes according to the international standard 10-20 system for dataset IIIa and dataset IIa, respectively. Thirty-two electrodes and eighteen electrodes marked red were selected for multiple-class motor imagery detection, respectively.

B. SIGNAL PREPROCESSING

Previous studies have reported that the dominant frequency bands related to motor imagery were μ rhythms (7-12 Hz) and β rhythms (14-30 Hz) [23]–[26]. In this paper, the EEG signal in the range of 4 to 40 Hz selects the sub-band for the corresponding band-pass filtering [9], [10], [27], [28].

In the preprocessing, the spatial filtering of MI data adopts common average reference (CAR) [29]. In band pass filtering, we divided the frequency band into 2, 6, 10, 12 frequency bands with different ranges for band pass filtering. The value ranges of two frequency bands are 7-14 Hz and 14-30 Hz, and 6 frequency bands are 7-12 Hz, 12-17 Hz, 17-22 Hz, 22-27 Hz, 27-32 Hz, and 7-30 Hz. The value ranges of 10 frequency bands are 4-8 Hz, 8-12 Hz, 12-16 Hz, 16-20 Hz, 20-24 Hz, 24-28 Hz, 28-32 Hz, 32-36 Hz, 36-40 Hz, and 7-30 Hz. The value ranges of the 12 frequency bands are 7-12 Hz, 9-14 Hz, 11-16 Hz, 13-18 Hz, 15-20 Hz, 17-22 Hz, 19-24 Hz, 21-26 Hz, 23-28 Hz, 25-30 Hz, 27-32 Hz, and 7-30 Hz.

C. FEATURE EXTRACTION

First, we define the four classes of MI tasks as x_1, x_2, x_3, and x_4, respectively. Then the covariance model of multiple-class MI space is shown as following [29]:

$$R_i = \frac{x_i x_i^T}{trace(x_i x_i^T)}, \quad i = 1, 2, 3, 4 \tag{1}$$

where x_i represents the trial of each class in the entire dataset. The dimension of x_i is the number of channels $\times$ (time window $\times$ sampling frequency). By accumulating each class of experiments in the training set by (1), R_i obtained is the sum of the covariances of each class of trial in the training set.

The compound covariance matrix formula for CSP is as follows:

$$R_x = R_1 + R_2 + R_3 + R_4 \tag{2}$$

The singular value decomposition of covariance matrix R_x can be carried out as:

$$R_x = U_0 \Lambda_C U_0^T \tag{3}$$

where U_0 is the unitary matrix of principal components, and Λ_C is the diagonal matrix of eigenvalues. After calculating singular value decomposition of eigenvector and eigenvalue matrix, the transformation matrix of covariance matrix can be obtained:

$$P = {\Lambda_C}^{-1/2} {U_0}^T \tag{4}$$

For multiple-class MI, multiple-class of OVR-CSP modes (such as left hand) can be calculated as:

$$\widetilde{R}_1 = R_2 + R_3 + R_4 \tag{5}$$

Then we transform R_1 and R_1 into:

$$G_1 = PR_1P^T, \widetilde{G}_1 = P\widetilde{R}_1P^T \tag{6}$$

Furthermore, we do eigenvalue decomposition for G_1 and $\widetilde{G}_1$:

$$G_1 = U_1 \wedge_1 {U_1}^T, \widetilde{G}_1 = U_1 \widetilde{\wedge}_1 {U_1}^T \tag{7}$$

By combining the equation (1)-(7), we can get:

$$(P^T U_1)^T R_1 (P^T U_1) + (P^T U_1)^T \widetilde{R}_1 (P^T U_1) = I \tag{8}$$

We get the common eigenvector matrix U for R_1 and $\widetilde{R}_1$. Further, CSP projection matrix $V_1 = U_1^T P$ can be obtained. One trial of the EEG data matrix X_i projection is obtained. The selected features of left-hand MI can be obtained by the following formula:

$$M_1 = V_1 x_i, i = 1, 2, 3, 4 \tag{9}$$

M2, M3, and M4 can be obtained in the same way. In this paper, the first four pairs and the last four pairs of eigenvalues in the projection matrix were selected, and CSP filters are used for spatial filtering to form eight eigenvalues in each trial of the training dataset [30].

We carried out the aforementioned feature extraction for each frequency band after preprocessing. Finally, N frequency bands for each trial need $N \times 8$ CSP filters for feature extraction. Eight eigenvalues extracted from each frequency band are merged to form $N \times 8$ eigenvalues. After the features obtained by the CSP, we uniformly normalize them to better perform feature selection and classification.

D. FEATURE SELECTION

The F-score algorithm has a simple but effective advantage for evaluating the discriminative power of each feature in the feature set [31], [32]. F-score is used to sort and select the features. With this method, the features with the best classification effect are selected from the classification order. The optimal feature set that can achieve the best accuracy of classification is the optimal feature set selected by F-score.

Given train feature dataset samples $X_k, k = 1, 2, \ldots, n$. The number of positive and negative samples is N_+ and N_-, respectively. Then, the F-score of the fth feature of the dataset is defined as [33]:

$$F_f = \frac{\left(\bar{x}_f^{(+)} - \bar{x}_f\right)^2 + \left(\bar{x}_f^{(-)} - \bar{x}_f\right)^2}{\frac{1}{N_+ - 1}\sum_{k=1}^{n_+}\left(x_{k,f}^{(+)} - \bar{x}_f^{(+)}\right)^2 + \frac{1}{N_- - 1}\sum_{k=1}^{n_+}\left(x_{k,f}^{(-)} - \bar{x}_f^{(+)}\right)^2} \tag{10}$$

where, $\bar{x}_f, \bar{x}_f^{(+)}$, and $\bar{x}_f^{(-)}, f = 1, 2, \ldots, m$ are the mean value of the ith feature on the whole train dataset, the mean value on the positive dataset and the mean value on the negative dataset, respectively.

$\bar{x}_{k,f}^{(+)}$ is the eigenvalue of the fth feature of the sample point of the kth positive class, and $\bar{x}_{k,f}^{(-)}$ is the eigenvalue of the fth feature of the sample point of the kth negative class. The greater the value of F, the stronger the discrimination between the features in different classes.

E. CLASSIFICATION

SNN is proposed based on biological principles, which could simulate the connection and communication between neurons to the great extent. The spike neuron model is the mathematical abstraction of the real neuron, which shows good performance and strong robustness in some pattern recognition problems [13], [17], [34], [35]. Due to such advantage, SNN is used in this study to classify the optimal feature set of MI.

Since the Izhikevich (IZ) model has good performance between biological accuracy and calculation cost, it is selected for the realization of the neuron model. The description of the IZ model is illustrated by the following equations [15], [36]:

$$v' = \frac{k(v - v_r)(v - v_t) - u + I}{C} \tag{11}$$

$$u' = a\{b(v - v_r) - u\}$$

$$if\ v > v_{peak}, then\ v \leftarrow c, u \leftarrow u + d \tag{12}$$

where k represents the rheobase resistance, v_r represents resting membrane potential, v_t represents the instantaneous threshold potential, C and v respectively represent the membrane capacitance and the membrane potential, while v_{peak} represents the spike cutoff value, u represents the recovery current, I represents a vector of the input current to the neuron, a represents a recovery time constant, b represents the input resistance, the voltage reset value is expressed by c, and d represents the outwards minus inwards currents that affect the after-spike behavior of the model during the spike period [14], [15]. The parameters used in the SNN are shown in Table 2. The detailed structure of the model can be described in [37].

TABLE 2. Parameters of SNN.

Parameter	Value
k	0.7
v_r	-60
v_t	-40
v_{peak}	35
C	100
a	0.03
b	-2
c	-50
d	100

To produce the desired behavior in the output of the spiking neuron, we must adjust the synaptic weights of the model. In this regard, we use the cuckoo search algorithm as a learning strategy to train the spiking neural model, which corresponds to the training stage of the spiking neuron [36]. In this algorithm, each egg in the nest represents a solution, while the cuckoo egg represents a new solution. Its goal is to use new and potentially better solutions, not bad ones in the nest. The detailed description of the algorithm can be found in [38].

When a new solution $X^{(t+1)}$ is generated for a cuckoo i, a Levy flight is performed, The equation as follows:

$$X_i^{(t+1)} = X_i^{(t)} + \alpha \oplus Levy(\lambda) \tag{13}$$

where $\alpha > 0$ is the step size. Usually, we can use $\alpha = 1$. The product $\oplus$ represents entrywise multiplications.

The Levy flight essentially provides a random walk, and the random step size is obtained from Levy distribution:

$$Levy \sim u = t^{(-\lambda)} \tag{14}$$

which has an infinite variance with an infinite mean. In the long run, the random walk via Levy flight is more effective in exploring the search space because of its longer step length. Because this kind of walking is more effective in exploring search space, it can regulate the synaptic weights of spike neurons [36].

For the problem of MI recognition, let the optimal CSP feature set $S = \{X_i, n\}_{i=1}^{p}$ selected by feature selection be the p input patterns, where $n = 1, \ldots, N$ is the class to of

$X_i \in IR^k$. First, we need convert each input mode to the current input I. It should be noted that the spike neuron model is stimulated by the injection current I calculated from the input pattern, rather than by the input pattern $X_i \in IR^k$. Since synaptic weights of the model are directly connected to the input pattern $X_i \in IR^k$, the injection current generated by this input mode can be calculated as [36]:

$$I = \gamma \cdot X \cdot W \tag{15}$$

where $W_i \in IR^k$ is the synaptic weights set of the neuron model, and γ is a gaining factor that helps the neuron fire. This kind of conversion can convert multiple input modes from the same class into the same or similar current, and help neurons generate similar firing rates. Then during T ms, the spiking neuron is stimulated with the input current I, and the firing rate is calculated. These steps are used in each input pattern. Calculate the average firing rate of each class $AFR \in IR^N$ by obtained the firing rate of each input.

If the spiking neuron is trained, the class used to determine the unknown input pattern $\widetilde{X}$ belongs will be determined by the firing rates generated by each input pattern. As described in the following equation:

$$cl = arg \min_{n=1}^{N}(|AFR_n - fr|) \tag{16}$$

where the firing rate of the neuron model stimulated by input pattern $\widetilde{X}$ is fr.

It is very important to find a set of optimal the neuron model $\overleftarrow{w}$ synaptic weights to improve the accuracy of the spiking neuron. This needs to be adjusted by using the cuckoo search algorithm. Therefore, the current behavior needed to generate the model can be realized by finding a set of synaptic weights through the following fitness function:

$$f(\overleftarrow{w}, S) = 1 - performance(\overleftarrow{w}, S) \tag{17}$$

where $\overleftarrow{w}$ represents the synapse of the model, s is the optimal CSP feature set as a set of input patterns, and $performance(\overleftarrow{w}, S)$ is a function of identifying the accuracy of the number of correct classified divided by the total number of tested.

F. PERFORMANCE MEASURE

The measurement performance used in this paper is classification accuracy and kappa value, respectively. The classification accuracy can be expressed by the following formula [24]:

$$accuracy = \frac{C}{N} \cdot 100\% \tag{18}$$

where C is the number of correctly classified samples of the test set. N represents the total number of test set samples.

Kappa is often used to measure multi-class problems, which can be expressed as [14]:

$$kappa = \frac{p_0 - p_e}{1 - p_e} \tag{19}$$

where p_0 is the overall agreement of the test set, which is equal to the value of accuracy. p_e is the chance agreement probability value of the test set, which can be obtained by the following formula:

$$p_e = \frac{\sum_i a_i b_i}{N \times N}, i = 1, 2, 3, 4 \tag{20}$$

where a_i and b_i represent the sum of ith class real samples and ith class predicted samples of the confusion matrix, respectively. N is the total number of test set samples.

III. EXPERIMENTAL RESULTS

To assess the impact of the frequency bands on MI-BCI performance, we evaluated the CSP and FBCSP methods for the following cases:

1) CSP: For the time window optimization problem of two datasets, it has been studied in [20], [39], [40]. On this basis, we manually select the optimal time window of each subject. For the dataset IIIa of the BCI Competition III, the optimal time windows of K3b, K6b, and L1b are 0.5-4.0 s, 0.5-3.6 s, and 0.5-3.6 s, respectively. For the dataset IIa of the BCI Competition IV, the optimal time windows of A01-A09 are 0.5-3.7 s, 0.5-3.7 s, 0.5-3.9 s, 0.5-3.5 s, 0.5-3.9 s, 0.5-3.8 s, 0.5-3.8 s, 0.5-3.4 s, and 0.5-3.5 s, respectively. After choosing the optimal time window, each subject carries out 7-30 Hz broad frequency band band-pass filtering, and finally extracts 8 eigenvalues through CSP.

2) 2FBCSP: The same time windows were used. 16 eigenvalues were extracted from the frequency bands 7-14 Hz and 14-30 Hz.

3) 6FBCSP: The same time windows were used. 48 eigenvalues were extracted from six frequency bands 7-12 Hz, 12-17 Hz, 17-22 Hz, 22-27 Hz, 27-32 Hz, and 7-30 Hz.

4) 10FBCSP: The same time windows were used. 80 eigenvalues were extracted from ten frequency bands 4-8 Hz, 8-12 Hz, 12-16 Hz, 16-20 Hz, 20-24 Hz, 24-28 Hz, 28-32 Hz, 32-36 Hz, 36-40 Hz, and 7-30 Hz.

5) 12FBCSP: The same time windows were used. 96 eigenvalues were extracted from twelve frequency bands 7-12 Hz, 9-14 Hz, 11-16 Hz, 13-18 Hz, 15-20 Hz, 17-22 Hz, 19-24 Hz, 21-26 Hz, 23-28 Hz, 25-30 Hz, 27-32 Hz, and 7-30 Hz.

The topographical maps of FBCSP weights for K3b and A01 are shown in Fig. 2. The color bars indicate changes in weights. Red represents a high weight in the topographic map, and blue represents a low weight in the topographic map. When the subject performed the left-hand motor imagery, the weights on the right brain hemisphere were high (in red color). When the subject performed the right-hand motor imagery, the high weights were on the left brain hemisphere. When the subject performed the foot motor imagery, the high weights appeared on the central brain region. When the subject performed the tongue motor imagery, the high weights were shown around the outer brain region. It can be seen that the activation intensity and topographic map distribution are different between different tasks.

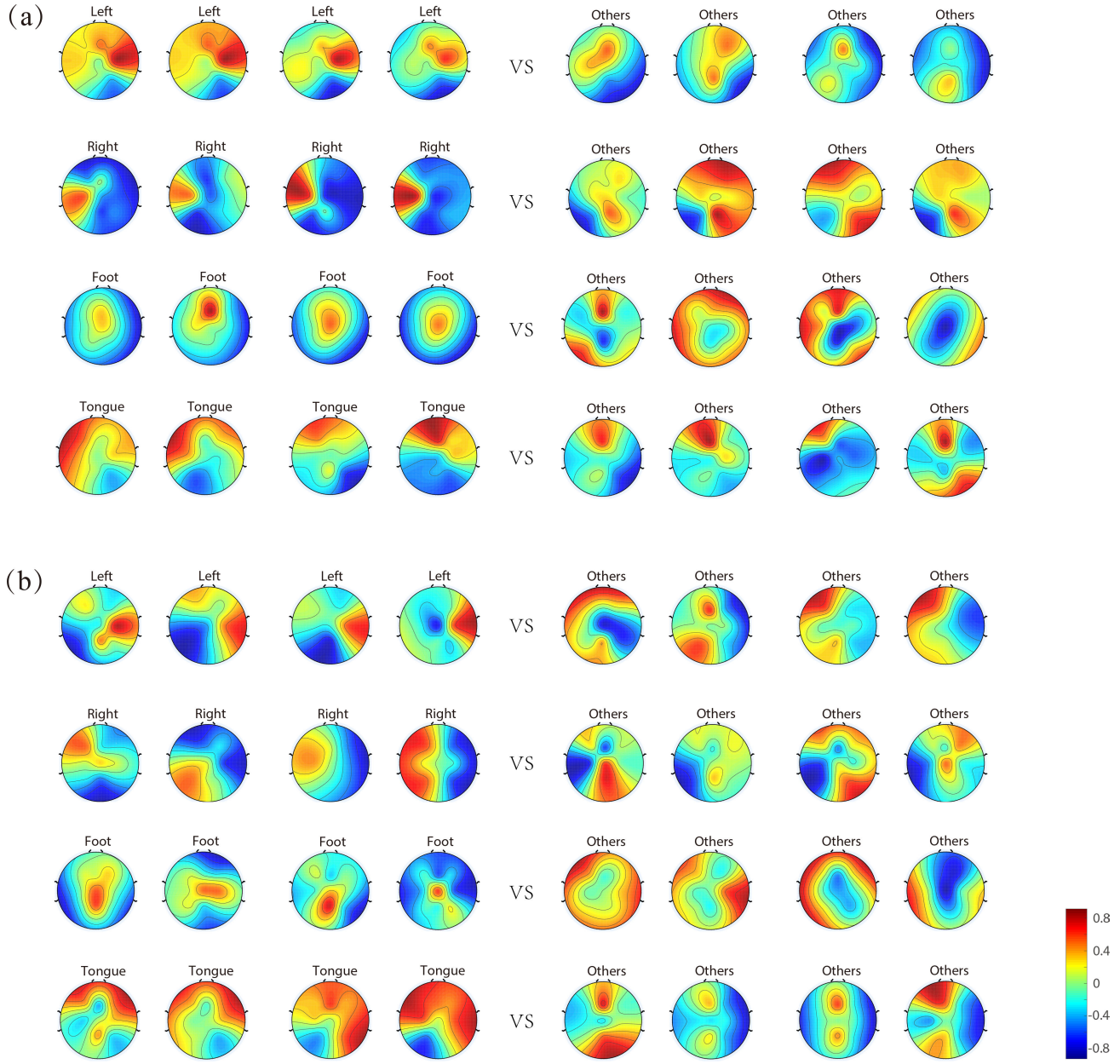

FIGURE 2. **(a). Topographies of FBCSP weights for subject K3b from dataset IIIa of BCI competition III. The first row to the fourth row are the topographies of OVR-FBCSP transformation matrix for the left hand motor imagery *vs* all other motor imageries (the rest), the right hand *vs* the rest, the foot *vs* the rest and tongue *vs* the rest, respectively. (b). Topographies of FBCSP weights for subject A01 from dataset IIa of the BCI Competition IV. The first row to the fourth row are the topographies of OVR-FBCSP transformation matrix for the left hand *vs* the rest, the right hand *vs* the rest, the foot *vs* the rest, and tongue *vs* the rest, respectively.**

These topographic map distributions verify the rationality of the subject's CSP projection matrix neurophysiology.

Since motor imagery of each limb part will cause the weight of the non-motor imagery cortex to decrease, CSP has a greater weight in the large area of the sensory motor cortex. Some areas that are not close to the sensory motor cortex also have larger weights, which may be caused by some artificial factor.

To date, most of researches on the MI classification addressed feature extraction and made relatively less attention on the development of classifier. Also, fixed frequency bands, fixed time windows, and all channels were used, which is time-consuming and is not optimal for the MI classification. In this paper, the OVR-FBCSP was used to extract the features of different time frames of different frequency bands of two datasets, and three classifiers (support vector machine (SVM), relevance vector machine (RVM), and SNN) were used for feature classification.

Table 3 showed that the accuracy of OVR-FBCSP-SNN was superior to the other methods in the assessment of the

TABLE 3. Accuracy comparison between the proposed SNN approach and the other methods on the dataset IIIa of the BCI Competition III and the dataset IIa of the BCI Competition IV.

Dataset	Sub.	Accuracy(%)														
		SVM					RVM					SNN				
		CSP	2FB	6FB	10FB	12FB	CSP	2FB	6FB	10FB	12FB	CSP	2FB	6FB	10FB	12FB
IIIa	K3b	90.00	93.89	95.56	95.00	**98.33**	91.11	92.22	93.89	93.33	97.78	86.67	91.67	97.22	94.44	96.11
	K6b	54.17	60.83	72.50	69.17	79.17	55.00	57.50	70.83	66.67	75.83	58.33	66.67	77.50	74.17	**82.50**
	L1b	76.67	82.50	86.67	83.33	87.50	74.17	80.83	84.17	80.00	85.83	75.00	83.33	89.17	85.00	**91.67**
	Average	73.61	79.07	84.91	82.50	88.33	73.43	76.85	82.96	80.00	86.48	73.33	80.56	87.96	84.54	**90.09**
IIa	A01	68.75	79.86	87.15	**90.28**	87.85	68.40	76.74	78.82	80.90	85.42	70.14	81.60	85.07	87.15	89.93
	A02	56.94	54.51	60.07	61.11	65.63	56.60	51.74	56.94	60.76	61.46	59.38	58.33	61.81	64.93	**68.06**
	A03	82.29	86.46	90.97	88.54	88.89	80.90	85.07	**92.01**	82.99	87.50	82.99	86.81	91.67	86.81	89.24
	A04	58.33	61.81	70.83	70.49	72.22	54.51	68.06	61.11	65.28	70.14	59.03	70.14	72.22	71.18	**74.31**
	A05	36.11	47.22	58.33	**74.31**	70.14	34.72	40.28	52.43	60.42	67.01	40.63	50.00	62.15	70.14	73.26
	A06	40.28	39.24	43.40	45.49	62.15	37.15	39.93	40.63	38.54	50.35	42.01	47.92	53.47	58.68	**66.32**
	A07	71.53	82.64	83.68	86.46	88.54	69.79	82.99	83.68	84.38	87.15	74.31	84.03	86.81	89.58	**91.32**
	A08	74.31	80.21	**89.58**	84.38	86.46	76.74	81.25	84.03	79.86	86.11	78.13	84.72	87.85	84.38	88.89
	A09	71.18	75.69	82.64	84.03	88.19	69.10	77.43	79.86	82.29	86.46	75.67	79.17	84.03	86.81	**90.63**
	Average	62.19	67.52	74.07	76.12	78.90	60.88	67.05	69.95	71.10	75.85	64.70	71.37	76.12	77.74	**81.33**

* 2FB, 6FB, 10FB and 12FB are the abbreviation of 2FBCSP, 6FBCSP, 10FBCSP and 12FBCSP, respectively.

TABLE 4. Kappa value comparison between the proposed SNN approach and the other methods on the dataset IIIa of the BCI Competition III and the dataset IIa of the BCI Competition IV.

Dataset	Sub.	Kappa														
		SVM					RVM					SNN				
		CSP	2FB	6FB	10FB	12FB	CSP	2FB	6FB	10FB	12FB	CSP	2FB	6FB	10FB	12FB
IIIa	K3b	0.866	0.919	0.941	0.933	**0.978**	0.882	0.896	0.919	0.911	0.970	0.822	0.889	0.963	0.926	0.948
	K6b	0.389	0.479	0.633	0.589	0.722	0.400	0.433	0.611	0.556	0.678	0.439	0.556	0.700	0.656	**0.767**
	L1b	0.689	0.767	0.822	0.778	0.833	0.656	0.744	0.789	0.733	0.811	0.666	0.778	0.855	0.800	**0.889**
	Average	0.648	0.721	0.799	0.767	0.844	0.646	0.691	0.773	0.733	0.820	0.643	0.741	0.839	0.794	**0.868**
IIa	A01	0.583	0.732	0.829	**0.870**	0.838	0.579	0.690	0.718	0.745	0.806	0.602	0.755	0.801	0.829	0.866
	A02	0.426	0.394	0.468	0.482	0.542	0.412	0.357	0.426	0.477	0.486	0.461	0.448	0.491	0.531	**0.574**
	A03	0.764	0.819	0.880	0.847	0.852	0.745	0.801	**0.894**	0.834	0.847	0.773	0.824	0.889	0.824	0.857
	A04	0.443	0.491	0.611	0.607	0.630	0.394	0.574	0.482	0.537	0.602	0.454	0.602	0.630	0.616	**0.657**
	A05	0.148	0.301	0.446	**0.657**	0.602	0.130	0.204	0.366	0.472	0.562	0.208	0.339	0.495	0.601	0.642
	A06	0.204	0.190	0.245	0.273	0.493	0.162	0.199	0.208	0.181	0.338	0.227	0.306	0.380	0.449	**0.551**
	A07	0.620	0.768	0.783	0.819	0.847	0.597	0.773	0.782	0.792	0.829	0.657	0.787	0.824	0.861	**0.884**
	A08	0.657	0.736	**0.862**	0.792	0.819	0.690	0.750	0.787	0.732	0.815	0.708	0.796	0.838	0.792	0.852
	A09	0.613	0.676	0.769	0.787	0.843	0.588	0.699	0.732	0.764	0.820	0.676	0.722	0.787	0.824	**0.875**
	Average	0.495	0.567	0.655	0.682	0.718	0.478	0.561	0.599	0.615	0.678	0.529	0.620	0.682	0.703	**0.751**

* 2FB, 6FB, 10FB and 12FB are the abbreviation of 2FBCSP, 6FBCSP, 10FBCSP and 12FBCSP, respectively.

dataset IIIa of BCI competition III for all subjects except the subject K3b. On average, the highest mean accuracy (90.09%) was achieved by OVR-12FBCSP-SNN. In the assessment of the dataset IIa of BCI competition IV, SNN was better than SVM and RVM in the overall classification of nine subjects. The highest accuracy of OVR-SNN was higher than that of OVR-SVM and OVR-RVM except for A01, A03, A05, and A08 subjects. In particular, the highest average accuracy of OVR-12FBCSP-SNN was 81.33%.

TABLE 5. The average training and testing time cost of the proposed method.

Datasets	Categories	Methods	Train	Test
			Total time/s	Total time/ms
Dataset IIIa	4	OVR-CSP-SNN	18.255	0.562
		OVR-2FBCSP-SNN	165.476	1.128
		OVR-6FBCSP-SNN	500.975	3.386
		OVR-10FBCSP-SNN	725.813	5.647
		OVR-12FBCSP-SNN	889.357	6.781
Dataset IIa	4	OVR-CSP-SNN	35.363	1.226
		OVR-2FBCSP-SNN	323.241	2.459
		OVR-6FBCSP-SNN	926.078	7.425
		OVR-10FBCSP-SNN	1170.510	12.438
		OVR-12FBCSP-SNN	1433.781	14.964

Table 4 showed the kappa values of all subjects. Except for the subject K3b, the kappa values of OVR-FBCSP-SNN in other subjects superior to the other methods in the assessment of the dataset IIIa of BCI competition III. The highest average kappa value (0.868) was achieved by OVR-12FBCSP-SNN. In the assessment of the dataset IIa of BCI competition IV, the overall kappa values of SNN in nine subjects were better than that of SVM and RVM. The highest average kappa value of OVR-12FBCSP-SNN was 0.751.

Table 5 showed the training and testing time of two datasets in different frequency band selection range. We can see with the increase of frequency bands number, the corresponding training and testing time also increases.

IV. DISCUSSION

In recent years, great progress has been made in the analysis of MI based on EEG signals, and the mechanism of different MI has gradually been revealed. In this paper, we explored the combinations of FBCSP and SVM, RVM, SNN for multiple-class MI classification. First, we used different time windows according to different subjects. And the corresponding band-pass filtering is carried out for each subject according to the same sub-band selection. Then, we extracted the CSP features in each frequency band and selected features. Finally, different classifiers were used to classify MI. Table 3 and Table 4 showed that the OVR-FBCSP-SNN was effective and feasible. These results were discussed in details below.

A. TIME WINDOWS FOR SPATIAL PATTERNS

A fixed time window (0.5-2.5 *s* with respect to the onset of cues) was usually used in the CSP for feature extraction [44], [45]. This is not very reasonable because the temporal course of brain activity responding to motor imagery is not exact the same and varies from one subject to another. In this study, the optimal time window was manually set for different subjects so that the classification accuracy was improved. For the dataset IIIa of the BCI Competition III, the optimal time windows of K3b, K6b, and L1b are 0.5-4.0 *s*, 0.5-3.6 *s*, and 0.5-3.6 *s*, respectively. For the dataset IIa of the BCI Competition IV, the optimal time windows of A01-A09 are 0.5-3.7 *s*, 0.5-3.7 *s*, 0.5-3.9 *s*, 0.5-3.5 *s*, 0.5-3.9 *s*, 0.5-3.8 *s*, 0.5-3.8 *s*, 0.5-3.4 *s*, and 0.5-3.5 *s*, respectively.

TABLE 6. Comparison of the proposed SNN approach with other approaches on the dataset IIIa of the BCI Competition III.

Methods	Accuracy(%)				Kappa
	Subject			Average	
	K3b	K6b	L1b		
Islam et al. [41]	95.30	69.20	83.30	82.60	-
Guan et al*. [42]	91.67	75.00	81.67	82.78	-
Mahmood et al. [20]	93.30	77.50	85.80	85.50	-
Selim et al. [39]	98.89	77.50	83.33	86.57	0.821
Masood et al. [21]	98.89	78.33	93.33	90.18	-
Sreeja et al*. [28]	94.94	90.46	90.12	91.84	0.920
He et al. [43]	85.00	94.00	100.00	93.00	-
OVR-CSP-SNN	86.67	58.33	75.00	73.33	0.643
OVR-2FBCSP-SNN	91.67	66.67	83.33	80.56	0.741
OVR-6FBCSP-SNN	97.22	77.50	89.17	87.96	0.839
OVR-10FBCSP-SNN	94.44	74.17	85.00	84.54	0.794
OVR-12FBCSP-SNN	96.11	82.50	91.67	90.09	0.868

* In these papers, training set and testing set are mixed to use k-fold cross validation.

B. DIFFERENT FREQUENCY RANGE SELECTION

Most of studies focused on the band selection of CSP filters [54]–[56]. Through the average division of different frequency bands, the CSP feature extraction is carried out for each sub-band, and then the optimal CSP feature combination in each sub-band is selected through feature selection. The

TABLE 7. Comparison of the proposed SNN approach with other approaches on the dataset IIa of the BCI Competition IV.

Methods	Accuracy(%)										Kappa
	Subject									Average	
	A01	A02	A03	A04	A05	A06	A07	A08	A09		
She et al. [46]	81.14	49.86	78.02	63.33	44.03	49.44	81.11	81.49	81.38	67.76	0.570
Zhao et al. [22]	72.00	49.00	82.00	58.00	70.00	54.00	77.00	79.00	80.00	69.00	0.583
Yang et al*. [47]	77.14	49.82	80.41	53.88	65.47	48.70	81.37	84.39	82.29	69.27	-
Sakhavi et al. [48]	87.50	65.28	90.28	66.67	62.50	45.49	89.58	83.33	79.51	74.46	0.659
Selim et al. [39]	90.56	66.32	91.99	70.28	68.53	55.75	90.63	87.80	85.07	78.55	0.714
Ai et al*. [49]	82.80	65.50	87.90	77.60	72.40	70.70	82.80	87.90	89.70	79.70	0.730
Kumar et al*. [50]	90.04	73.30	92.50	82.72	71.68	64.98	85.01	86.74	81.90	80.99	0.743
Razi et al. [51]	83.33	69.09	88.89	79.17	75.00	68.06	85.42	89.24	90.97	81.02	0.750
Liyanage et al. [52]	95.40	64.20	96.80	67.20	75.90	65.20	78.10	96.10	93.10	81.48	-
Zhang et al. [53]	89.00	69.00	92.00	82.00	84.00	68.00	95.00	90.00	92.00	84.00	0.800
Xu et al. [40]	85.71	78.57	92.15	95.67	89.20	85.12	79.23	81.28	80.67	85.59	0.766
OVR-CSP-SNN	70.14	59.38	82.99	59.03	40.63	42.01	74.31	78.13	75.67	64.70	0.530
OVR-2FBCSP-SNN	81.60	58.33	86.81	70.14	50.00	47.92	84.03	84.72	79.17	71.41	0.620
OVR-6FBCSP-SNN	85.07	61.81	91.67	72.22	62.15	53.47	86.81	87.85	84.03	76.12	0.682
OVR-10FBCSP-SNN	87.15	64.93	86.81	71.18	70.14	58.68	89.58	84.38	86.81	77.74	0.703
OVR-12FBCSP-SNN	89.93	68.06	89.24	74.31	73.26	66.32	91.32	88.89	90.63	81.33	0.751

* In these papers, training set and testing set are mixed to use k-fold cross validation.

optimal CSP feature combination is classified to get a good classification effect.

The experimental results showed that the FBCSP combined with SNN was an effective method to improve the accuracy of MI classification [27]. Ang *et al.* used the FBCSP combined with various feature selection and classifiers to identify the two-class MI. The results showed that the FBCSP is superior to other feature extraction methods [7]. Mahmood *et al.* used the FBCSP combined with SVM to classify multiple-class MI. Compared with other methods, this method obtained the best recognition accuracy [20]. Zhang *et al.* used OVR-FBCSP combined with CNN+LSTM method for MI recognition [53]. Islam *et al.* used TSM to find the precise frequency band associated with the MI mission for MI recognition [41]. In their work, the optimal MI recognition accuracy based on the sub-band selection method of mutual information is 82.6%±13.06, which is lower than our experimental result 90.09% and proves that the effect of FBCSP is feasible for MI recognition.

C. DIFFERENT CLASSIFIERS IN MOTOR IMAGERY

For the classification of MI features, the classifier has a great influence on the classification effect. In this study, we use SVM, RVM, and SNN as classifiers and apply the feature selection method of F-score to screen the most distinctive CSP features in each subject, to help improve the accuracy of recognition. For the dataset IIIa of the BCI competition III and dataset IIa of BCI competition IV, the average accuracy of the OVR-FBCSP-SNN classifier is 90.09% and 81.33%, respectively. This result proves that SNN is a good classifier based on EEG, and our classification method is feasible and effective.

Referring to other MI literature, Liu *et al.* used features to define a score use the step-wise linear discriminant analysis (SWLDA) method performing MI classification [57]. Nguyen *et al.* used CSP for feature extraction and fuzzy logic system (FLS) for classification. CSP is used to extract significant features, and then these features are input into FLS as classification input [58]. G. S. *et al.* used Bayesian networks and artificial neural networks to classify MI features [59]. Yang *et al.* designed a classification method called adaptive kernel fisher support vector machine (KF-SVM) is designed and applied to EEG MI classification in BCI [60]. Komijani *et al.* presents MI classification for BCI systems using a recurrent adaptive neuro-fuzzy interface system (ANFIS), and the classification system is based on time-series prediction [61]. Lahiri *et al.* proposed to use the whole classifier composed of the k-nearest neighbor (KNN) layer for classification [62].

D. COMPARISON OF DIFFERENT MOTOR IMAGERY RELATED STUDIES

Obviously, compared with other recent methods (Table 6 and Table 7), our proposed OVR-FBCSP-SNN method has some advantages. The accuracy and kappa value of the two datasets are close to the highest value of the latest literature. The

results show that the framework can be used as an alternative method.

E. EXPERIMENTAL LIMITATIONS AND FUTURE CONSIDERATIONS

First of all, the dataset of MI is limited to the left hand, right hand, foot, and tongue, which cannot reflect other situations of MI. For example, grabbing, lifting, and other forms of MI are not included in the dataset. In the future, we will realize the recognition of MI with more classes of MI. Secondly, we select the optimal time window and frequency band of each subject manually, which is not an effective method in practical application. It is urgent to improve the use of automatic selection of each subject's optimal time window and frequency band, which is efficient and accurate. Thirdly, we only use SNN as classifier without considering whether it can be used as a feature extraction method.

V. CONCLUSION

To enhance the performance of multiple-class MI classification, a new method of combining one-vs-rest filter bank common spatial pattern with spiking neural networks was proposed. Two datasets of four classes of MI (dataset IIIa of BCI competition III and dataset IIa of BCI competition IV) were used to evaluate the proposed method. Experimental results demonstrated that our method was comparable to the best existing method in terms of classification accuracy. It demonstrated that the proposed method could serve as an alternative for multi-class MI classification.

ACKNOWLEDGMENT

(Hongtao Wang and Cong Tang contributed equally to this work.)

REFERENCES

[1] V. A. Maksimenko, S. A. Kurkin, E. N. Pitsik, V. Y. Musatov, A. E. Runnova, T. Y. Efremova, A. E. Hramov, and A. N. Pisarchik, "Artificial neural network classification of motor-related EEG: An increase in classification accuracy by reducing signal complexity," *Complexity*, vol. 2018, pp. 1–10, Aug. 2018.

[2] W. Zgallai, J. T. Brown, A. Ibrahim, F. Mahmood, K. Mohammad, M. Khalfan, M. Mohammed, M. Salem, and N. Hamood, "Deep learning AI application to an EEG driven BCI smart wheelchair," in *Proc. Adv. Sci. Eng. Technol. Int. Conf. (ASET)*, Mar. 2019, pp. 1–5.

[3] B. Xu, Z. Wei, A. Song, C. Wu, D. Zhang, W. Li, G. Xu, H. Li, and H. Zeng, "Phase synchronization information for classifying motor imagery EEG from the same limb," *IEEE Access*, vol. 7, pp. 153842–153852, 2019.

[4] Y. Lu, Y. Hu, R. Liu, H. Wang, H. Asama, and F. Duan, "The design of simulation vehicle system controlled by multichannel EEG based on imaginary movements," in *Proc. 35th Chin. Control Conf. (CCC)*, Jul. 2016, pp. 4976–4981.

[5] S. Lemm, B. Blankertz, G. Curio, and K.-R. Muller, "Spatio-spectral filters for improving the classification of single trial EEG," *IEEE Trans. Biomed. Eng.*, vol. 52, no. 9, pp. 1541–1548, Sep. 2005.

[6] G. Dornhege, B. Blankertz, M. Krauledat, F. Losch, G. Curio, and K.-R. Müller, "Combined optimization of spatial and temporal filters for improving brain-computer interfacing," *IEEE Trans. Biomed. Eng.*, vol. 53, no. 11, pp. 2274–2281, Nov. 2006.

[7] K. Keng Ang, Z. Yang Chin, H. Zhang, and C. Guan, "Filter bank common spatial pattern (FBCSP) in brain-computer interface," in *Proc. IEEE Int. Joint Conf. Neural Netw. IEEE World Congr. Comput. Intell.*, Jun. 2008, pp. 2390–2397.

[8] K. P. Thomas, C. Guan, C. Tong Lau, A. P. Vinod, and K. K. Ang, "A new discriminative common spatial pattern method for motor imagery brain–computer interfaces," *IEEE Trans. Biomed. Eng.*, vol. 56, no. 11, pp. 2730–2733, Nov. 2009.

[9] Y. Zhang, G. Zhou, J. Jin, X. Wang, and A. Cichocki, "Optimizing spatial patterns with sparse filter bands for motor-imagery based brain–computer interface," *J. Neurosci. Methods*, vol. 255, pp. 85–91, Nov. 2015.

[10] V. Peterson, D. Wyser, O. Lambercy, R. Spies, and R. Gassert, "A penalized time-frequency band feature selection and classification procedure for improved motor intention decoding in multichannel EEG," *J. Neural Eng.*, vol. 16, no. 1, Feb. 2019, Art. no. 016019.

[11] Q. Yu, H. Tang, K. C. Tan, and H. Yu, "A brain-inspired spiking neural network model with temporal encoding and learning," *Neurocomputing*, vol. 138, pp. 3–13, Aug. 2014.

[12] H. Sossa, J. M. Antelis, and L. E. Falcón, "Motor imagery task classification in eeg signals with spiking neural network," in *Proc. Mex. Conf. Pattern Recognit.*, 2019, pp. 14–24.

[13] S. Dora, K. Subramanian, S. Suresh, and N. Sundararajan, "Development of a self-regulating evolving spiking neural network for classification problem," *Neurocomputing*, vol. 171, pp. 1216–1229, Jan. 2016.

[14] C. D. Virgilio G., J. H. Sossa A., J. M. Antelis, and L. E. Falcón, "Spiking neural networks applied to the classification of motor tasks in EEG signals," *Neural Netw.*, vol. 122, pp. 130–143, Feb. 2020.

[15] R. I. Carino-Escobar, J. Cantillo-Negrete, J. Gutierrez-Martinez, and R. A. Vazquez, "Classification of motor imagery electroencephalography signals using spiking neurons with different input encoding strategies," *Neural Comput. Appl.*, vol. 30, no. 4, pp. 1289–1301, Aug. 2018.

[16] A. N. Niranjani and M. Sivachitra, "Motor imagery signal classification using spiking neural network," in *Proc. Int. Conf. Intell. Sustain. Syst. (ICISS)*, Dec. 2017, pp. 901–904.

[17] R. Salazar-Varas and R. A. Vazquez, "Evaluating spiking neural models in the classification of motor imagery EEG signals using short calibration sessions," *Appl. Soft Comput.*, vol. 67, pp. 232–244, Jun. 2018.

[18] G. Pfurtscheller and A. Schlögl. *BCI Competition III Dataset IIIa*. [Online]. Available: http://www.bbci.de/competition/iii/

[19] C. Brunner, R. Leeb, G. Müller-Putz, A. Schlögl, and G. Pfurtscheller. *BCI Competition 2008—Graz Data Set A*. [Online]. Available: http://www.bbci.de/competition/iv/

[20] A. Mahmood, R. Zainab, R. B. Ahmad, M. Saeed, and A. M. Kamboh, "Classification of multi-class motor imagery EEG using four band common spatial pattern," in *Proc. 39th Annu. Int. Conf. IEEE Eng. Med. Biol. Soc. (EMBC)*, Jul. 2017, pp. 1034–1037.

[21] N. Masood, H. Farooq, and I. Mustafa, "Selection of EEG channels based on spatial filter weights," in *Proc. Int. Conf. Commun., Comput. Digit. Syst. (C-CODE)*, Mar. 2017, pp. 341–345.

[22] D. Zhao, F. Tang, B. Si, and X. Feng, "Learning joint space-time-frequency features for EEG decoding on small labeled data," *Neural Netw.*, vol. 114, pp. 67–77, Jun. 2019.

[23] K. A. Ludwig, R. M. Miriani, N. B. Langhals, M. D. Joseph, D. J. Anderson, and D. R. Kipke, "Using a common average reference to improve cortical neuron recordings from microelectrode arrays," *J. Neurophysiol.*, vol. 101, no. 3, pp. 1679–1689, Mar. 2009.

[24] J. Li and L. Zhang, "Active training paradigm for motor imagery BCI," *Exp. Brain Res.*, vol. 219, no. 2, pp. 245–254, Jun. 2012.

[25] J. Li and L. Zhang, "Bilateral adaptation and neurofeedback for brain computer interface system," *J. Neurosci. Methods*, vol. 193, no. 2, pp. 373–379, Nov. 2010.

[26] J. Li, Z. Struzik, L. Zhang, and A. Cichocki, "Feature learning from incomplete EEG with denoising autoencoder," *Neurocomputing*, vol. 165, pp. 23–31, Oct. 2015.

[27] P. Bustios and J. L. Rosa, "Restricted exhaustive search for frequency band selection in motor imagery classification," in *Proc. Int. Joint Conf. Neural Netw. (IJCNN)*, May 2017, pp. 4208–4213.

[28] S. R. Sreeja and D. Samanta, "Classification of multiclass motor imagery EEG signal using sparsity approach," *Neurocomputing*, vol. 368, pp. 133–145, Nov. 2019.

[29] H. Wang, T. Li, A. Bezerianos, H. Huang, Y. He, and P. Chen, "The control of a virtual automatic car based on multiple patterns of motor imagery BCI," *Med. Biol. Eng. Comput.*, vol. 57, no. 1, pp. 299–309, Jan. 2019.

[30] B. Blankertz, R. Tomioka, S. Lemm, M. Kawanabe, and K.-R. Müller, "Optimizing spatial filters for robust EEG single-trial analysis," *IEEE Signal Process. Mag.*, vol. 25, no. 1, pp. 41–56, Dec. 2008.

[31] Q. Song, H. Jiang, and J. Liu, "Feature selection based on FDA and F-score for multi-class classification," *Expert Syst. Appl.*, vol. 81, pp. 22–27, Sep. 2017.
[32] J. Gao, Z. Wang, Y. Yang, W. Zhang, C. Tao, J. Guan, and N. Rao, "A novel approach for lie detection based on F-Score and extreme learning machine," *PLoS ONE*, vol. 8, no. 6, 2013, Art. no. e64704.
[33] W. Huang, H. Yan, R. Liu, L. Zhu, H. Zhang, and H. Chen, "F-score feature selection based Bayesian reconstruction of visual image from human brain activity," *Neurocomputing*, vol. 316, pp. 202–209, Nov. 2018.
[34] N. Kasabov and E. Capecci, "Spiking neural network methodology for modelling, classification and understanding of eeg spatio-temporal data measuring cognitive processes," *Inf. Sci.*, vol. 294, pp. 565–575, Feb. 2015.
[35] A. Taherkhani, A. Belatreche, Y. Li, and L. P. Maguire, "A supervised learning algorithm for learning precise timing of multiple spikes in multilayer spiking neural networks," *IEEE Trans. Neural Netw. Learn. Syst.*, vol. 29, no. 11, pp. 5394–5407, Nov. 2018.
[36] R. A. Vazquez, "Training spiking neural models using cuckoo search algorithm," in *Proc. IEEE Congr. Evol. Comput. (CEC)*, Jun. 2011, pp. 679–686.
[37] E. Izhikevich, "Dynamical systems in neuroscience: The geometry of excitability and bursting," *Applied Mathematical Sciences*. Cambridge, MA, USA: MIT Press, 2007.
[38] X.-S. Yang and S. Deb, "Cuckoo search via Lévy flights," in *Proc. World Congr. Nature Biol. Inspired Comput. (NaBIC)*, Dec. 2009, pp. 210–214.
[39] S. Selim, M. M. Tantawi, H. A. Shedeed, and A. Badr, "A CSP/AM-BA-SVM approach for motor imagery BCI system," *IEEE Access*, vol. 6, pp. 49192–49208, 2018.
[40] B. Xu, L. Zhang, A. Song, C. Wu, W. Li, D. Zhang, G. Xu, H. Li, and H. Zeng, "Wavelet transform time-frequency image and convolutional network-based motor imagery EEG classification," *IEEE Access*, vol. 7, pp. 6084–6093, 2019.
[41] M. R. Islam, T. Tanaka, and M. K. I. Molla, "Multiband tangent space mapping and feature selection for classification of EEG during motor imagery," *J. Neural Eng.*, vol. 15, no. 4, Aug. 2018, Art. no. 046021.
[42] S. Guan, K. Zhao, and S. Yang, "Motor imagery EEG classification based on decision tree framework and Riemannian geometry," *Comput. Intell. Neurosci.*, vol. 2019, pp. 1–13, Jan. 2019.
[43] L. He, B. Liu, D. Hu, Y. Wen, M. Wan, and J. Long, "Motor imagery EEG signals analysis based on Bayesian network with Gaussian distribution," *Neurocomputing*, vol. 188, pp. 217–224, May 2016.
[44] S. Kumar, K. Mamun, and A. Sharma, "CSP-TSM: Optimizing the performance of Riemannian tangent space mapping using common spatial pattern for MI-BCI," *Comput. Biol. Med.*, vol. 91, pp. 231–242, Dec. 2017.
[45] L. Song and J. Epps, "Classifying EEG for brain-computer interface: Learning optimal filters for dynamical system features," *Comput. Intell. Neurosci.*, vol. 2007, pp. 1–11, 2007.
[46] Q. She, B. Hu, Z. Luo, T. Nguyen, and Y. Zhang, "A hierarchical semi-supervised extreme learning machine method for EEG recognition," *Med. Biol. Eng. Comput.*, vol. 57, no. 1, pp. 147–157, Jan. 2019.
[47] H. Yang, S. Sakhavi, K. Keng Ang, and C. Guan, "On the use of convolutional neural networks and augmented CSP features for multi-class motor imagery of EEG signals classification," in *Proc. 37th Annu. Int. Conf. IEEE Eng. Med. Biol. Soc. (EMBC)*, Aug. 2015, pp. 2620–2623.
[48] S. Sakhavi, C. Guan, and S. Yan, "Learning temporal information for brain-computer interface using convolutional neural networks," *IEEE Trans. Neural Netw. Learn. Syst.*, vol. 29, no. 11, pp. 5619–5629, Nov. 2018.
[49] Q. Ai, A. Chen, K. Chen, Q. Liu, T. Zhou, S. Xin, and Z. Ji, "Feature extraction of four-class motor imagery EEG signals based on functional brain network," *J. Neural Eng.*, vol. 16, no. 2, Apr. 2019, Art. no. 026032.
[50] S. Udhaya Kumar and H. Hannah Inbarani, "PSO-based feature selection and neighborhood rough set-based classification for BCI multiclass motor imagery task," *Neural Comput. Appl.*, vol. 28, no. 11, pp. 3239–3258, Nov. 2017.
[51] S. Razi, M. R. Karami Mollaei, and J. Ghasemi, "A novel method for classification of BCI multi-class motor imagery task based on Dempster–Shafer theory," *Inf. Sci.*, vol. 484, pp. 14–26, May 2019.
[52] S. R. Liyanage, C. Guan, H. Zhang, K. K. Ang, J.-X. Xu, and T. H. Lee, "Dynamically weighted classification with clustering to tackle non-stationarity in brain computer interfacing," in *Proc. Int. Joint Conf. Neural Netw. (IJCNN)*, Jun. 2012, pp. 1–6.
[53] R. Zhang, Q. Zong, L. Dou, and X. Zhao, "A novel hybrid deep learning scheme for four-class motor imagery classification," *J. Neural Eng.*, vol. 16, no. 6, 2019, Art. no. 066004.
[54] K. K. Ang, Z. Y. Chin, C. Wang, C. Guan, and H. Zhang, "Filter bank common spatial pattern algorithm on BCI competition IV datasets 2a and 2b," *Frontiers Neurosci.*, vol. 6, p. 39, 2012.
[55] S. Kumar, A. Sharma, and T. Tsunoda, "An improved discriminative filter bank selection approach for motor imagery EEG signal classification using mutual information," *BMC Bioinf.*, vol. 18, no. S16, p. 545, Dec. 2017.
[56] S. Kumar and A. Sharma, "A new parameter tuning approach for enhanced motor imagery EEG signal classification," *Med. Biol. Eng. Comput.*, vol. 56, no. 10, pp. 1861–1874, Oct. 2018.
[57] K. Liu, Y. Yu, Y. Liu, and Z. Zhou, "Eeg-based motor imagery differing in task complexity," in *Proc. Int. Conf. Intell. Sci. Big Data Eng.*, Sep. 2017, pp. 608–618.
[58] T. Nguyen, I. Hettiarachchi, A. Khosravi, S. M. Salaken, A. Bhatti, and S. Nahavandi, "Multiclass EEG data classification using fuzzy systems," in *Proc. IEEE Int. Conf. Fuzzy Syst. (FUZZ-IEEE)*, Jul. 2017, pp. 1–6.
[59] G. S. Sagee and S. Hema, "EEG feature extraction and classification in multiclass multiuser motor imagery brain computer interface u sing Bayesian network and ANN," in *Proc. Int. Conf. Intell. Comput., Instrum. Control Technol. (ICICICT)*, Jul. 2017, pp. 938–943.
[60] B. Yang, C. Fan, J. Jia, S. Chen, and J. Wang, "Adaptive KF-SVM classification for single trial EEG in BCI," in *Proc. Adv. Comput. Methods Life Syst. Modeling Simulation*, 2017, pp. 35–45.
[61] H. Komijani, M. R. Parsaei, E. Khajeh, M. J. Golkar, and H. Zarrabi, "EEG classification using recurrent adaptive neuro-fuzzy network based on time-series prediction," *Neural Comput. Appl.*, vol. 31, no. 7, pp. 2551–2562, Jul. 2019.
[62] R. Lahiri, A. Rakshit, and A. Konar, "Discriminating motor imagery EEG signals using an improvised regularised CSP algorithm," in *Proc. IEEE 1st Int. Conf. Power Electron., Intell. Control Energy Syst. (ICPEICES)*, Jul. 2016, pp. 1–6.

HONGTAO WANG (Member, IEEE) received the Ph.D. degree in pattern recognition and intelligent systems from the South China University of Technology, in 2015.

He is currently a Full Professor with the Faculty of Intelligent Manufacturing, Wuyi University, and been selected as a Thousand-Hundred-Ten Talent of Universities in Guangdong Province. He is also the Director of the Jiangmen Brain-like Computation and Hybrid Intelligence Research and Development Center. From January 2017 to January 2019, he was a Visiting Research Fellow with the Centre for Life Sciences, National University of Singapore. His current research interests include the fields of brain-like computation, pattern recognition, deep learning, and hybrid intelligence.

CONG TANG was born in Hunan, China, in 1995. He received the bachelor's degree from the School of Xingxiang, Xiangtan University, China, in 2017. He is currently pursuing the master's degree with the Faculty of Intelligent Manufacturing, Wuyi University. His research interests include pattern recognition and brain–machine interface.

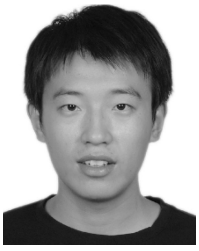

TAO XU received the Ph.D. degree from the Department of Biomedical Engineering, City University of Hong Kong, in 2019. He joined Wuyi University as a Distinguished Professor. His research interest includes computational neuroscience and neural prosthetic systems.

TING LI received the B.S. degree in automatic control from the Taiyuan Machinery College, China, in 1984, the M.S. degree in control theory and control engineering from Northwestern Polytechnical University, Xian, China, in 1994, and the Ph.D. degree in mechanical and electrical engineering from the Beijing Institute of Technology, Beijing, China, in 2002.

Since 2002, he has been a Professor with the School of Information Engineering, Wuyi University of Technology. His research interests include pattern recognition and signal processing.

LINFENG XU was born in Guandong, China, in 1994. He received the bachelor's degree from the School of Guangdong University of Petrochemical Technology, China, in 2017. He is currently pursuing the master's degree with the Faculty of Intelligent Manufacturing, Wuyi University. From 2017 to 2019, he involved in algorithm research and development in Shenzhen. His research interests include pattern recognition and brain like computation.

HONGWEI YUE received the Ph.D. degree in control theory and control engineering from the Guangdong University of Technology, China, in 2013. He is currently an Associate Professor with the Faculty of Intelligent Manufacturing, Wuyi University, China. His research interests include image processing, biomedical instrument, and information security.

PENG CHEN was born in Guangdong, China, in 1979. He received the B.S. degree from the School of Electronics and Information, South China University of Technology, Guangzhou, in 2001, and the Ph.D. degree in electronic circuit and system from the South China University of Technology, in June 2006.

Since July 2006, he has been a Lecturer with the School of Information Engineering, Wuyi University of Technology. His research interests include measurement, signal processing, and automatic control.

JUNHUA LI (Senior Member, IEEE) received the Ph.D. degree in computer science from the Department of Computer Science and Engineering, Shanghai Jiao Tong University, China, in 2013.

He is currently a Lecturer with the School of Computer Science and Electronic Engineering, University of Essex, Colchester, U.K. He was a Senior Research Fellow with the National University of Singapore, Singapore. His research interests include brain–computer interface, computational neuroscience, data analytics, and machine learning.

ANASTASIOS BEZERIANOS (Senior Member, IEEE) received the degree in physics from Patras University, the degree in telecommunications from Athens University, and the Ph.D. degree in bioengineering from the University of Patras. He is currently the Head of the Cognitive Engineering (COGEN) Laboratory, N.1 Health Institute, National University of Singapore, a Professor with the NUS Graduate School for Integrative Sciences and Engineering, and a Visiting Professor with the Computer Science Department, New South Wales University (NSWU), Canberra, ACT, Australia. He has been a Professor of medical physics with the Medical School of Patras University, Patras, Greece, since 2004. His research entails diverse areas spanning from artificial intelligence and robotics to biomedical signal processing and brain imaging as well as mathematical biology and systems medicine and bioinformatics. His work is summarized in 140 journals and 217 conference proceedings publications, one book, and two patents. He has research collaborations with research institutes and universities in Japan, China, and Europe. He is also a Fellow of the European Alliance for Medical and biological Engineering and Science (EAMBES), and the Founder and the Chairman of the Biannual International Summer School on Emerging Technologies in biomedicine. He is also an Associate Editor of the IEEE TRANSACTIONS ON NEURAL SYSTEMS AND REHABILITATION ENGINEERING (TNSRE), the *PLOS ONE*, and *Neuroscience Journal* and a Reviewer for several international scientific journals. He is also a Registered Expert of the Horizon 2020 Program of the European Union and a Reviewer of research grant proposals in Greece, Italy, Cyprus, and Canada.